# DRY FRICTION BACKWARD WHIRL OF ROTORS: THEORY, EXPERIMENTS, RESULTS, AND RECOMMENDATIONS

**Alexander R. Bartha**
International Center for Magnetic Bearings, ETH Zurich, Switzerland
bartha@ifr.mavt.ethz.ch, rotordynamics@yahoo.com

## ABSTRACT
This paper presents a theoretical and experimental study into the dry friction backward whirl of rotors. A model is derived that is able to describe the behaviour of a rotor from an excitation up to and including fully established backward whirl. A test rig is presented with which these processes were studied experimentally for a rotor running in conventional (ball-)bearings up to a rotational frequency of 166 Hz (10'000 rpm). Test results are presented and discussed. These results include the whirl behaviour of a rotor in both a very heavy and a stator with compliant mountings and the influence of different system parameters on the whirl behaviour. The numerical predictions are compared to the measured results. Recommendations are given on how to avoid dry friction backward whirl.

## INTRODUCTION
Dry friction backward whirl is a state of motion, in which a rotor, after a sufficiently strong initial excitation, runs on the inner surface of its stator. This motion is driven by the frictional force between the rotor and the stator, which acts in the direction opposite to the direction of rotation. Backward whirl is a rare event but due to the very high frequencies and forces occurring, it can have fatal consequences for the affected plant. Rosenblum [9] reports the complete destruction of a 600 MW turbo generator by backward whirl.
Backward whirl can occur in rotor systems running in conventional bearings if contact with the stator is enforced by a sufficiently large disturbance. It can also occur in systems running in active magnetic bearings (AMBs) after a breakdown of the magnetic forces or in case of overload. For all plants, however, the present quest for achieving high efficiency by using narrow clearances increases the risk of frictional contact between the rotor and the stator and brings with it the danger of backward whirl.
In the literature, only a very limited number of research articles on backward whirl can be found. Only some authors, when modelling backward whirl, take into account the finite stiffness of the stator [2], [3], [6], [8], [10]. Few papers report experimental work, [3], [7], and except for [4], [5], and [10], the system parameters are usually greatly idealised and not representative for real systems. [4] and [5] report measurements on AMB-supported rotors whirling in retainer bearings at high rotational velocities. Despite these publications, the phenomenon of backward whirl is still not really understood and there remain many open questions, especially associated with whirl in plants with realistic parameters, such as speed of rotation, clearances, eigenfrequencies, and seal elements. Therefore this work pursues the following aims: firstly, to provide a sound theoretical and experimental knowledge of backward whirl in realistic systems and secondly, to give recommendations concerning how to assess the risk of backward whirl for a given plant, how to avoid backward whirl and how to alleviate its consequences, if necessary. This work mainly deals with rotors running in conventional bearings, but the findings could easily be generalised for plants with AMBs. For a far more detailed presentation of this work, the reader is referred to [1].

## MODELLING BACKWARD WHIRL
### The General Model
Firstly a general model is presented that describes all major effects occurring from the excitation of the rotor, during impact with the stator, up to fully established backward whirl. For modelling the individual phases,

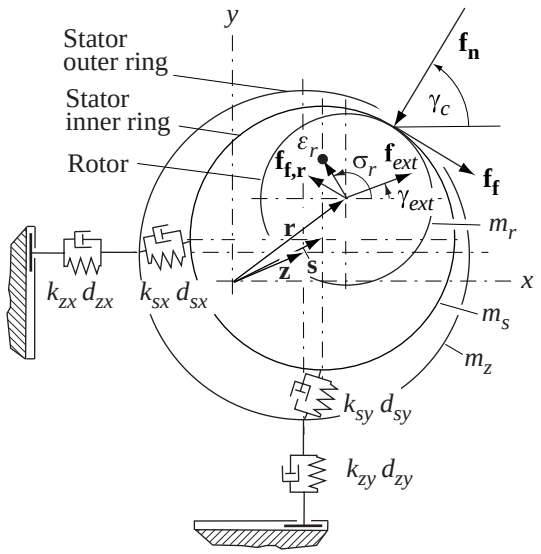


**FIGURE 1:** Whirl model incorporating a Jeffcott rotor and a stator consisting of two nested masses. Boldface variables represent vectors with *x* and *y* components.

potential simplifications are then introduced and discussed.

For the rotor, we assume a non-gyroscopic Jeffcott rotor with viscous damping, with or without imbalance $\varepsilon_r$. The stator is represented by a compliant structure consisting of two nested rings, taking into account up to two vibrational modes. Figure 1 gives the structure of this model together with the used variables and the contact forces acting on the rotor. During contact between the rotor and the stator, a very small contact deformation $x_c$ in the radial direction is admitted[1]. For the calculation of the contact normal force $f_n$ a linear visco-elastic contact law is used[2]: $f_n = k_c x_c + d_c \dot{x}_c$ with local contact stiffness $k_c$ and local contact damping $d_c$. For the calculation of the frictional force acting between the rotor and the stator, we use Coulomb's friction model with the coefficient of friction $\mu$, which links the frictional force $f_f$ to the normal force $f_n$: $f_f = \mu f_n$. $\mu$ is a function of the relative sliding velocity $v_{rel,s}$ at the point of contact at least in the sense that the direction of the frictional force reverses when $v_{rel,s}$ changes its sign. Furthermore, we consider the rolling frictional force with the coefficient $\mu_r$: $f_{f,r} = \mu_r f_n$ , which, strictly speaking, is a function of the direction of the relative tangential velocity of the rotor and the stator. No tangential contact damping force is taken into account since it is assumed to be already included in the coefficient of friction, $\mu$. An external excitation force acting on the rotor, $f_{ext}$ , is also taken into account.

In the following, *r*, *s*, and *z* as variables or subscripts denote displacements or properties of the rotor, the inner stator ring and the outer stator ring, respectively. *m*, *J*, *d*, and *k* are the mass, rotational inertia, damping coefficient, and the stiffness of a body, while *x* and *y* mark the direction of displacement. The subscript *c* denotes a contact property, as in $\gamma_c$ , which is the angle of contact between the rotor and the stator. With the angle of rotation $\sigma_r$ , the rotational velocity $\omega_{rot}(t)$, the torque of the drive $t_d$ , the rotor's radius at the contact location, $R_r$ , and after some minor simplifications, for the case of contact between the rotor and the stator inner ring we derive the following equations of motion:

$$m_r\ddot{r}_x + d_r\dot{r}_x + k_r r_x = -f_n\cos(\gamma_c) + f_{ext}\cos(\gamma_{ext}) + \ldots$$
$$(\mu - \mu_r) f_n \sin(\gamma_c) + \ldots$$
$$m_r\varepsilon_r\ddot{\sigma}_r \sin(\sigma_r) + m_r\varepsilon_r\dot{\sigma}_r{}^2\cos(\sigma_r) \qquad (2.1)$$

$$m_r\ddot{r}_y + d_r\dot{r}_y + k_r r_y = -f_n\sin(\gamma_c) + f_{ext}\sin(\gamma_{ext}) - \ldots$$
$$(\mu - \mu_r) f_n \cos(\gamma_c) - \ldots$$
$$m_r\varepsilon_r\ddot{\sigma}_r\cos(\sigma_r) + m_r\varepsilon_r\dot{\sigma}_r{}^2\sin(\sigma_r) \qquad (2.2)$$

$$m_s\ddot{s}_x + d_{sx}\dot{s}_x + k_{sx}s_x = f_n\cos(\gamma_c) - \ldots$$
$$(\mu - \mu_r) f_n \sin(\gamma_c) + d_{sx}\dot{z}_x + k_{sx}z_x \qquad (2.3)$$

$$m_s\ddot{s}_y + d_{sy}\dot{s}_y + k_{sy}s_y = f_n\sin(\gamma_c) + \ldots$$
$$(\mu - \mu_r) f_n \cos(\gamma_c) + d_{sy}\dot{z}_y + k_{sy}z_y \qquad (2.4)$$

$$m_z\ddot{z}_x + (d_{zx} + d_{sx})\dot{z}_x + k_{zx}z_x = d_{sx}\dot{s}_x + k_{sx}s_x \qquad (2.5)$$

$$m_z\ddot{z}_y + (d_{zy} + d_{sy})\dot{z}_y + k_{zy}z_y = d_{sy}\dot{s}_y + k_{sy}s_y \qquad (2.6)$$

$$\ddot{\sigma}_r(t) = \dot{\omega}_{rot}(t) = \frac{t_d - \mu f_n R_r}{J_r} \qquad (2.7)$$

For $f_n$ we find: $f_n = k_c A + d_c B$ with

$$A = \sqrt{(r_x - s_x)^2 + (r_y - s_y)^2} - c \qquad (2.8)$$

$$B = \frac{(r_x - s_x)(\dot{r}_x - \dot{s}_x) + (r_y - s_y)(\dot{r}_y - \dot{s}_y)}{\sqrt{(r_x - s_x)^2 + (r_y - s_y)^2}} \qquad (2.9)$$

[1] A different way to model the contact between the rotor and the stator is to suppose a kinematic motion of the rotor on the stator's inner surface with no allowed contact deformation. The equations of motion can then be formulated using an algebraic constraint for the rotor's position or a formulation in minimal co-ordinates [1]. The equations of motion are then only valid for continuous contact, impacts or the rotor's free flight phase cannot be modelled. This method was first used by Black [2], who generally described the dynamics of the rotor and the stator by transfer functions and studied their behaviour under kinematic contact. He found periodic whirl motions, which impose upper limits on the whirl frequency, irrespective of the rotor's initial speed of rotation. This theory is not presented here, in the results section however, some remarks will be given on its validity when compared to numerical and experimental findings.

[2] For special configurations of the impacting bodies, a non-linear contact model may also be used.

If there is no contact between the rotor and the stator, the contact forces are zero.

**The Onset Phase of Backward Whirl**

The phase from an excitation acting on the rotor until it either makes continuous contact with the stator or re-enters a damped free vibration will be referred to here as onset phase of backward whirl. The most important information concerning this phase is how robust a given rotor is against excitation.

In the following, we neglect a potential imbalance of the rotor and assume the stator to be concentric and rigid. This is appropriate since during the onset phase the contact forces are not very high so that for most systems any displacement of the stator can be neglected[3]. Excitations acting on the rotor are brought to a common base by considering only the magnitude and orientation of the impact velocity with which the rotor first contacts the stator. Every time the rotor impacts the stator, its normal velocity component decreases whereas the tangential velocity component in the whirl direction increases. The increase is determined by the impact velocity, the elasticity of the impact, and the coefficient of friction. This behaviour is mainly accumulative since, during the free flight phases, not much energy can be drawn from the rotor's lateral motion. From quite simple considerations we find the critical tangential velocity in the whirl direction, $v_{t,crit}$. For tangential velocities above $v_{t,crit}$, the frictional force between the rotor and the stator outweighs the rotor's viscous damping force and further accelerates the whirl. $v_{t,crit}$ is mainly determined by the rotor's first eigenfrequency and the coefficient of friction [1].

An impact of the rotor with the stator which just leads to a tangential velocity in the whirl direction of $v_{t,crit}$ is called a critical impact. It is clear that an impact in the whirl direction more easily triggers backward whirl than a velocity vector in the opposite direction. From simulation however it can be seen that a radial impact is very close to the worst case since it can give raise to further impacts which further increase the rotor's tangential velocity. This is why we study the critical radial impact velocity $v_{r,crit}$, which we define as the minimum radial impact velocity at which a given rotor must impact its stator so that it just undergoes backward whirl motion. $v_{r,crit}$ represents an excellent measure for the robustness of a given plant against excitation. If $v_{r,crit}$ is computed as a function of a system parameter, the result can be interpreted as a stability map with respect to the bearable excitation. In this work, $v_{r,crit}$ was calculated numerically for different configurations of the test rig and compared to experimental findings.

**Established Backward Whirl**

After the rotor made continuous contact with its stator, backward whirl inevitably develops. The frictional force accelerates the rotor into the whirl direction, which leads to an increase in the centrifugal force and consequently the frictional force. When studying established backward whirl, the most important factor is the whirl frequency $\omega_{wh}$, in particular its maximum value $\omega_{wh,max}$, since this determines the maximum acting forces and the frictional torque. The predicted value of $\omega_{wh,max}$ is strongly dependent on the chosen whirl model.

The simplest possible model is that of a rotor whirling in a completely rigid stator. Here the acceleration of the whirl would not stop until the rotor rolls on the inner surface of the stator, *i.e.* when the relative sliding velocity at the contact location disappears. From this, we find: $\omega_{wh,max} = \omega_{rot} \cdot R_r / c$, with the parameters as defined above. Even if we assume that during whirl no energy is transmitted from the drive and that rolling takes place at a greatly reduced rotational velocity, for usual plants, the notion of a rigid stator cannot be preserved [1]. Therefore, we have to take into account the dynamic properties of the stator and their influences on the whirl motion by using the whirl model presented in equations (2.1) to (2.9). These equations of motion were evaluated numerically using MATLAB for a variety of parameter sets and compared to experimental findings. The significant variables were the rotor's and stator's displacements, the frequencies of these motions, and the acting forces. The simulations serve both the purpose of clarifying the test results and to predict the whirl motions for new systems.

## TEST RIG AND EXPERIMENTS

In order to study backward whirl experimentally, a test rig was built to represent a small turbo compressor. It mainly consisted of a Jeffcott type rotor running in conventional self-aligning ball bearings. The rotor was equipped with a disk of diameter 200 mm that was either solid or fitted with radial seal elements. The rotor length was 947 mm; the total mass was approximately 12 kg. Its first eigenfrequency was about 45 Hz, which corresponds to a first critical speed of 2'700 rpm. An external damping appliance could be mounted to the rotor that increased its modal damping from 0.3 % to about 3.5 %. The rotor was driven by a 2 kW electric asynchronous motor, equipped with a frequency converter for variable rotational speed up to a maximum of 250 Hz (15'000 rpm). Power was transmitted via a flexible electromagnetic coupling that could be released before the measurement sequence was initiated. The

[3] For lightweight shells, as used in aero-engine applications, the stator's compliance however should already be taken into account for the calculation of the onset phase.

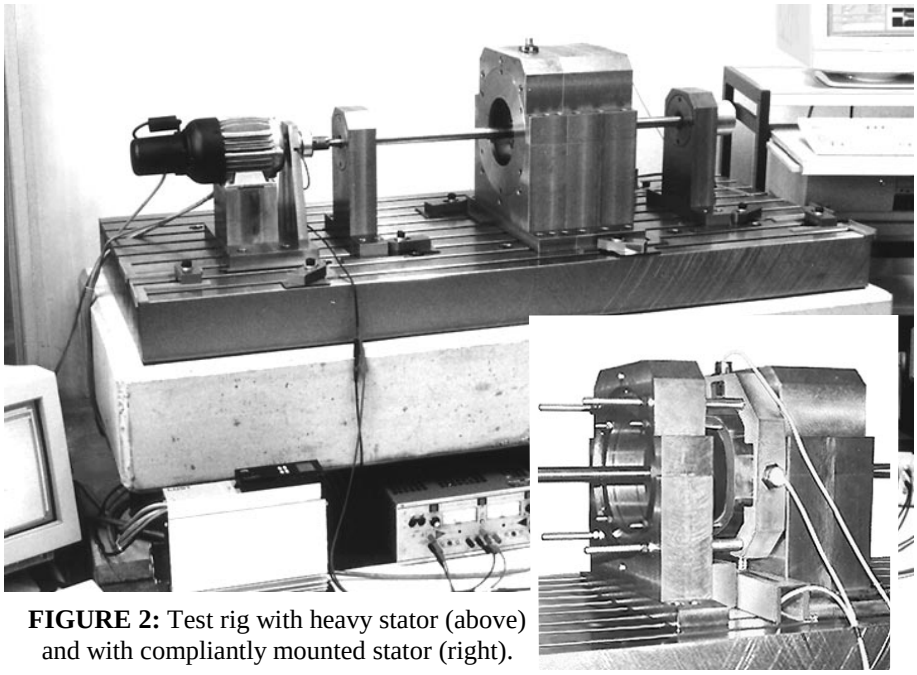

**FIGURE 2:** Test rig with heavy stator (above) and with compliantly mounted stator (right).

rotor was running in a stator with a radial clearance of 0.2 mm. Two stators could be selected for the experiments, one weighing 300 kg and rigidly fixed, the other a ring of about 10 kg and compliantly mounted with a first (translational) eigenfrequency of about 60 Hz. The most significant feature of the test rig was a single AMB that was not used to suspend the rotor but to apply a defined excitation to the rotor. The AMB was mounted near the centre of the rotor's span to provide maximum influence on the first bending mode. Its maximum force was about 1'500 N. With this AMB a variety of different excitation patterns could be simulated. The test rig was equipped with displacement sensors at the approximate location of the disk and an optical encoder to provide accurate information about the rotor's current speed of rotation. Additional displacement sensors and accelerometers were added when needed. The data acquisition was done via a PC-based system consisting of an A/D converter card and the commercial software Lab-VIEW. The test rig was mounted on a one-ton steel mounting plate and a one-ton steel reinforced concrete foundation. The whole test rig was supported by four spring damper elements. Figure 2 shows a photograph of the system with heavy stator (large picture) and with compliantly mounted stator (small inset). The test rig was carefully mounted and the sensors were calibrated.

With this test rig a variety of tests on backward whirl was performed. The tests were carried out to determine the critical radial impact velocity and the general behaviour during whirl as functions of various system parameters. To this aim, the rotor was excited by radial impacts to the stator with steadily increasing velocity. The excitation in every experiment was removed before the rotor impacted the stator so that only its free vibration was studied. From the sampled data, the actual impact velocity was determined. From the last test that did not lead to whirl and the first one that triggered whirl, the critical radial impact velocity was determined. The data for those tests that lead to whirl were evaluated with respect to the rotor's and stator's displacements, frequencies, and other variables. Most of the tests were performed using the rotor fitted with a solid disk. These tests were performed at rotational velocities ranging from 15 Hz (900 rpm) up to 166 Hz (10'000 rpm). In additional tests, the behaviour of a rotor fitted with seal elements was studied and the influence of a compliant stator mounting on the whirl behaviour was investigated.

## RESULTS

### The Onset Phase of Backward Whirl

**Test Results.** In order to trigger backward whirl, the rotor was usually accelerated in the radial direction towards the stator. When the initial impact velocity was below a certain limit, the rotor made one or more impacts and then entered a damped free vibration without further contacts to the stator. When the impact velocity was above this limit, the rotor, after several contacts, gained enough tangential velocity to make continuous contact with the stator and began backward whirl motion. This limit velocity, which for a first radial impact was defined as the critical radial impact velocity $v_{r,crit}$ was non-ambiguous and the rotor's behaviour was reproducible. The number of impacts was usually low and ranged from one to five. No major unexpected effects were found in the rotor's motion and the compliance of the heavy stator was negligible during this phase. The dependence of the critical impact velocity on various system parameters, for the heavy stator set up, was determined experimentally for five different configurations. For the standard rotor with a solid disk, the mean value of $v_{r,crit}$ after 26 tests was 0.093 m/s. When the modal damping for the same rotor was increased from 0.3 % to 3.5 %, $v_{r,crit}$ increased to

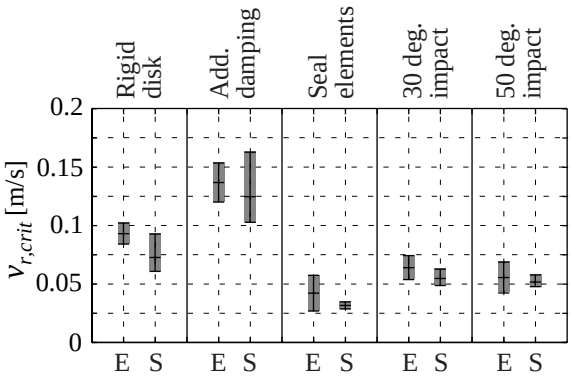


**FIGURE 3:** Comparison of experimental (E) and simulation (S) results for the critical radial impact velocity for different configurations of the test rig.

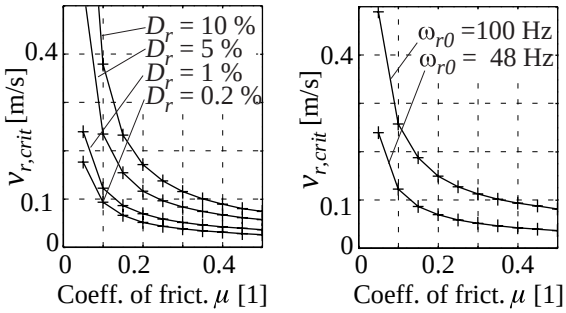


**FIGURE 4:** Simulation results for the critical radial velocity $v_{r,crit}$ as a function of different system parameters.

0.137 m/s. $v_{r,crit}$ for the rotor fitted with seal elements was only 0.043 m/s. When the impact was inclined into the whirl direction by 30 degrees, the critical impact velocity dropped to 0.064 m/s, for an impact inclined by 50 degrees, the critical value was only 0.056 m/s.

**Simulation Results.** The presented results were used to assess the validity of the model for the onset phase of backward whirl. For the test rig, the system parameters such as the coefficient of friction or the contact parameters for the above-described configurations were determined independently and the critical impact velocities were calculated. Figure 3 gives a comparison of the experimental and numerical values. For each case, the expected value of the experimental series is given together with the confidence interval +/- 1.9*s*, where *s* is the standard deviation of the respective set of measurements. The confidence intervals for the calculations were obtained by varying the coefficient of friction by +/- 25 %. We see that the numerical results are in excellent agreement with the experimental values: not only is the influence of all parameters represented correctly, but also the absolute values of the critical velocities are matched.

From simulation, we find that, although there are many parameters influencing a plant's stability, the most important one is the coefficient of friction between the rotor and the stator. For the rotor fitted with seal elements, a very high coefficient of friction at the metal sheet's tips most likely was the cause for the very high readiness to enter whirl motion. Other important parameters (see figures 3 and 4) are the rotor's modal damping and its first eigenfrequency, which determines the critical tangential velocity $v_{t,crit}$. As a result it can be stated that the simple model used here is very suitable to calculate the system's robustness against excitation.

**Established Backward Whirl**

**General Test Results.** When the rotor made continuous contact with the stator, its behaviour in all cases was very similar and distinct phases of the motion could be observed. Figure 5 shows the rotor's orbit for a whirl started at an initial rotational velocity of 40 Hz (2'400 rpm). The phases can also be seen in figure 6, which gives the rotor's *x* displacement and rotational velocity as functions of time. Initially, no excitation was acting on the rotor and it was executing an orbit imposed by imbalance (1). When the AMB performed impact excitation, the rotor was accelerated (2) until it hit the stator for the first time (3). After a short series of impacts (4) the rotor made continuous contact with the stator (5) and, driven by the friction force, the whirl motion accelerated very rapidly until the whirl frequency and the rotor's displacement reached a maximum (6). At the same time, the rotation was decelerated by the frictional torque. After that, the whirl frequency decelerated very rapidly (7). For a short time the rotor still stayed in contact with the stator, whirling at a considerably lower, but still rather high frequency (8). Finally, the rotor lost contact with the stator and entered a damped free vibration with decreasing amplitude (9).

**Test at 40 Hz (2'400 rpm).** In the 40 Hz (2'400 rpm) test, he rotor's whirl frequency accelerated from about 55 Hz at the beginning of the whirl up to a maximum of about 530 Hz. This maximum was achieved only 0.1 s after the excitation and was kept for three to four revolutions. At the same time, the rotor was rapidly decelerated by the acting frictional torque; it took only 0.012 s to bring the rotor to a standstill. The rotational velocity was very low at the time of the maximum whirl frequency, approximately 2 Hz (120 rpm). The rotor's maximum amplitude at the time of the highest whirl frequency was considerably larger than the annular clearance. This can mainly be attributed to the compliance of the stator relative to the AMB block, that housed the sensors, and to some tilting of the rotor

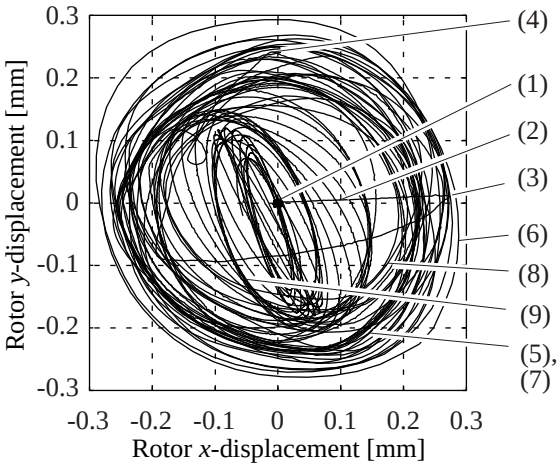


**FIGURE 5:** Rotor orbit during whirl started at a rotational velocity of 40 Hz (2'400 rpm). The different phases of motion are described in the text.

between the disk and the sensor location. The deformation of the disk at the contact location was negligible compared to these effects. The maximum displacements of the stator were in the order of magnitude of about +/-0.05 mm, which is much higher than had been expected. After about 20 whirl tests the contacting surfaces were slightly damaged. The surfaces were flattened, small pits were present and there was a thin film of abraded material. With respect to the high number of violent whirls however, the damage was surprisingly low.

**Test at 166 Hz (10'000 rpm).** Whirl tests were performed at rotational velocities ranging up to 166 Hz (10'000 rpm). The results of these tests were very similar to the tests at low rotational velocities and all the different phases of the whirl motion described above could also be observed in these tests. The maximum whirl frequencies were about 400 Hz and did not exceed the values determined at lower rotational velocities. However, the high-speed tests differed from the low-speed tests with respect to mainly two attributes. Firstly, the excitation that was needed to trigger whirl was considerably higher than in the other tests. Secondly, the duration of the whirl was very long: it took nearly 0.8 s to decelerate from 166 Hz (10'000 rpm) to standstill. During this time, there were intervals where the whirl frequency dropped as low as 100 Hz. Both of these effects can be explained by a strong reduction of the coefficient of friction due to the high tangential velocity. For the onset phase, this effect most likely stems from the property of dry friction to decrease with increasing sliding velocity at least in a certain range of speeds. For established whirl, the reduction in the coefficient of friction most likely stems from the very high power dissipation in the contact surfaces that leads to local

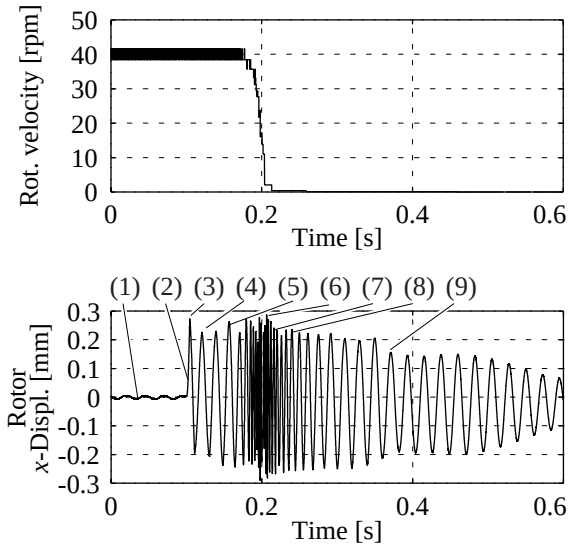


**FIGURE 6:** Rotational velocity and *x* displacement of the rotor during whirl started at a rotational velocity of 40 Hz (2'400 rpm). The different phases of motion are described in the text.

melting of the contacting bodies. The assumption of local melting was verified by the wear observed: the surfaces of the rotor and the stator were found to be burned at the contact location.

**Test with Seal Elements.** Whirl tests were performed at rotational velocities of 20 Hz (1'200 rpm) to 40 Hz (2'400 rpm) using a disk fitted with seal elements. The rotor's behaviour for the 20 Hz (1'200 rpm) and 30 Hz (1'800 rpm) cases was very similar to the case with the rigid disk. After the test at 30 Hz (1'800 rpm) an enlargement of the annular clearance could be observed. During the 40 Hz (2'400 rpm) test the seal elements bent and collapsed. The rotor was deflected until it touched the retainer bearings.

**Test with a compliant stator.** In order to check the influence of the additional compliance of the stator on the whirl behaviour and to investigate the possibility of low frequency whirl motions as predicted by Black [2], tests were performed using the compliant stator set up as described above. During whirl, two distinct whirl frequencies could be found in the rotor's and stator's motions. One was a low frequency, high amplitude motion at about 50 Hz, the other was a superimposed high frequency, low amplitude motion at about 400 Hz. It was clearly visible that the 400 Hz whirl motion was dominant with respect to the acting forces and torque and that the rotor's deceleration was only determined by this motion. The rotor's and stator's displacements were very large and reached values of more than 1 mm. After the whirl, the stator was twisted and the rods on which the stator ring was supported were severely bent. This

observation is in good agreement with the high whirl frequencies and the acting frictional torque.

**Simulation Results.** The whirl model presented above, equation (2.1) to (2.9), was successively evaluated with the parameters of the test rig for different levels of simplification. As predicted, the model assuming a completely rigid stator was in no way able to represent the established whirl motion. The predicted maximum whirl frequencies were too high by factors of 10 to 50, even if it was supposed that no energy was transmitted to the rotor once whirl started. The use of a more complex model, where the stator was represented by one mass with two degrees of freedom, improved the modelling. However, the predicted whirl frequencies were still much higher than the measured ones. The full model, taking into account two vibrational modes of the stator, was able to adequately represent the rotor's and stator's behaviour during fully established backward whirl. Since the determination of the dynamic system parameters posed some problems, for this model the stator's masses, stiffnesses and damping coefficients were adapted to yield best results[4]. For the calculation it was required that the maximum displacements of the outer stator ring did not exceed the measured values. The displacements of the stator inner ring were not restricted. The calculation results match the measurements very well. All of the characteristic phases of backward whirl can be determined from simulation. With the parameters given below, a maximum whirl frequency of about 660 Hz was calculated. Figure 7 gives a detailed comparison of the experimental and simulation results about the maximum whirl frequency as a function of the rotor's initial rotational velocity. It can be seen that the numerical results are in very good agreement with the experimental findings. The maximum whirl frequency both in experiment and in simulation first increases with an increasing rotational velocity of the rotor but soon reaches a maximum that is not exceeded even if the rotational velocity is increased further. This behaviour is represented very well by simulation. From the parameters used in the simulation

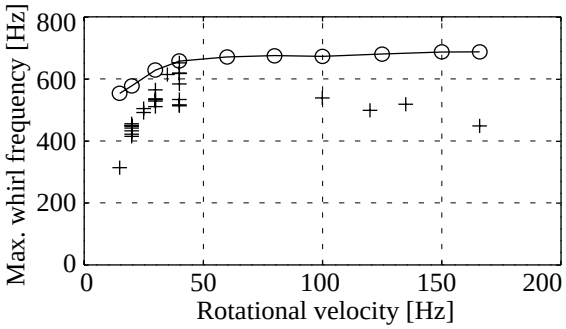


**FIGURE 7**: Maximum whirl frequencies as a function of the initial rotational velocity. Experiments (crosses) *vs.* simulation (circles and lines).

it can be calculated that the maximum whirl frequency corresponds to the first eigenfrequency of the coupled rotor-stator system[5]. Minor deviations from this value are due to the anisotropy in the model. From 100 Hz (6'000 rpm) on, the experimentally determined values decrease again. This is due to the strongly decreasing coefficient of friction due to the melting of the contacting surfaces. The time to bring the rotor to a standstill for rotational frequencies up to 40 Hz (2'400 rpm) was comparable to the time measured. For the high-speed tests however, the experimentally determined stopping time was much longer. This is also due to the low coefficient of friction.

The simulation results for the whirl in a compliantly mounted stator were very similar to the results for the rigid stator. Again, the maximum whirl frequency matched an eigenfrequency of the coupled system. We can state that for both systems the main influence on the rotor's behaviour comes from the stator's higher eigenmodes.

Without going into detail, it should be mentioned that using these models and a mathematical stability analysis, predictions made by Black's model [2] could be checked. It was found that the dominant impact of the system's eigenfrequencies on the whirl behaviour could be confirmed as well as the existence and stability of most of the proposed steady whirl motions. For the simple model, where the stator is represented by only one mass, however, Black's predictions are not accurate enough: the proposed periodic motions at the system's lowest coupled eigenfrequency turn out to be unstable. This is in agreement with the transient numeric integration and experimental results, where the whirl behaviour in the compliantly mounted stator was mainly governed by the stator ring's second (oval) mode.

Finally, it can be stated that the model proposed here takes into account all of the important effects influen-

[4] The parameter set that was used to represent the heavy stator assembly in most of the calculations was the following: $m_r$ = 10 kg, $k_r = 9.1 \cdot 10^5$ N/m, $d_r$ = 20.5 Ns/m, $m_s$ = 10 kg , $k_s = 8.9 \cdot 10^8$ N/m , $d_s$ = 28'300 Ns/m, $m_z$ = 10 kg, $k_z = 3.6 \cdot 10^9$ N/m, $d_z$ = 18'970 Ns/m, $c$ = 0.2 mm, $\mu$ = 0.15 , $\mu_r$ = 0.025 , $\varepsilon_r$ = 0. Additionally, an anisotropy in the stator's stiffness and damping in the $x$ and $y$ directions of +/-10 % was introduced in some calculations. The comparably low stator masses at first glance seem not to fit the very heavy stator, but are a good match with the determination from a finite-element calculation of the stator's static stiffness and the measured eigenfrequency.

[5] This is the system where the rotor is rigidly connected to the stator.

cing backward whirl and is very suitable to calculate the rotor's and stator's behaviour.

## CONCLUSIONS AND RECOMMENDATIONS

Dry friction backward whirl is a rare event but is feasible even in plants with realistic parameters, such as narrow clearances and high rotational velocities. Backward whirl can cause severe damage to a rotor or a plant in at least three ways. Firstly, since the location from which backward whirl originates is usually an annular seal location, the contact forces between the rotor and the stator can destroy the seal elements. Secondly, the rotor can reach large displacements even at locations different from that which the whirl originated from. This is caused by the high whirling frequencies and centrifugal forces. This may cause a permanent deformation of the rotor. Thirdly, the most severe threat to the integrity of the plant seems to be the frictional torque that can damage couplings or even shear the shaft.

The parameters that govern backward whirl are mainly the coefficient of friction for the onset phase and the eigenfrequencies of the system for established backward whirl. The rotor's rotational velocity does not have a major impact on the maximum whirl frequency or the violence of the whirl. To model the onset phase of backward whirl, a simple model assuming a rigid stator can usually be used. To model established whirl, the higher eigenmodes of the stator must be included. Black's model [2] in most cases gives correct results for the maximum whirl frequency.

With respect to the onset of backward whirl, it should not be taken for granted that occasional contact between the rotor and stator can be tolerated. Double-sided labyrinth seals may be used to increase the clearance gap between the seal element's tips and the opposing stationary element without sacrificing thermal efficiency. Most emphasis should be given to the reduction of the coefficient of friction between the rotor and the stator. A high stiffness of the shaft and high modal damping make the rotor robust against given excitation. For rotors suspended in AMBs, it's more complicated to prevent backward whirl, since there is no permanent restoring force exerted by the shaft. In any case, the reduction of the coefficient of friction between the rotor and the stator is of ultimate importance. The use of ball bearings as retainer bearings seems to be a good way to achieve this. In case the magnetic bearing is still in operation, *i.e.* for a temporary overload, the AMB can be used to counteract backward whirl. Since, in this case, the bearing force is not sufficient to prevent the rotor from touching the boundary, it does not make sense to use the entire load capacity for a radial restoring force. A much more reasonable approach for avoiding backward whirl is to exert tangential forces opposite to the whirl direction as soon as the rotor approaches the retainer bearings. If the rotor is bouncing in the retainer bearing, it seems to be more promising to exert damping forces rather than to try to re-centre the rotor.

One of the few approaches that seem to be promising to reduce the frequencies of established backward whirl is to design the contact area of the stator in a way that provides favourable dynamic properties. From the results of the present work however it can be stated that simply suspending the stator in a flexible manner will not necessarily bring down the whirl frequency to the rigid body eigenfrequency of the coupled system.

## REFERENCES

[1] Bartha, A. R.; *Dry Friction Backward Whirl of Rotors*; Doctoral Thesis, ETH Zürich, to be published in 2000

[2] Black, H. F.; *Interaction of a Whirling Rotor with a Vibrating Stator across a Clearance Annulus*; J. Mech. Eng. Sci., Vol. 10, Nr. 1, 1968

[3] Crandall, S. H.; *From Whirl to Whip in Rotordynamics*; Trans. ITFoMM, Third Internat. Conf. on Rotordynamics, Lyon, France, 1990

[4] Fumagalli, M.; Schweitzer, G.; *Motion of a Rotor in Retainer Bearings*; 5th Internat. Symp. on Magnetic Bearings, Kanazawa, Japan, 1996

[5] Fumagalli, M.; *Modelling and Measurement Analysis of the Contact Interaction between a High Speed Rotor and its Stator*; Doctoral Thesis ETH Zürich Nr. 12509, Zürich, 1997

[6] Kirk, R. G.; *Evaluation of AMB Turbomachinery Auxiliary Bearings*; Journal of Vibrations and Accoustics, Transactions of the ASME, Vol. 121, April 1999

[7] Lingener, A.; *Experimental Investigation of Reverse Whirl of a Flexible Rotor*; Trans. IFToMM, Third Internat. Conf. on Rotordynamics, Lyon, France, 1990

[8] Maslen, E. H.; Barrett, L. E.; *Feasible Whirl of Rotors in Auxiliary Bearings*; Proceedings of MAG '95, August 10-11 1995, Alexandria, Virginia

[9] Rosenblum, V. I.; *Entstehung mehrfacher Wellen-brüche nach dem Bruch einer Laufschaufel oder Radscheibe bei Dampfturbinen*; Allianz Report 68 (1995), Heft 5

[10] *A Seminar on Modern Analysis and Testing Tools for Rotating Machinery Dynamics: A Survey on the Results of the BRITE-Programs ROSTADYN and MARS*; Imp. College, London, June 14, 1996